Solid-State NMR Investigations of Molecular Dynamics in Polyphenylene Dendrimers: Evidence of Dense-Shell Packing

M. Wind,[†] K. Saalwächter,*[,‡] U.-M. Wiesler,[†] K. Müllen,[†] and H. W. Spiess*[,†]

Max-Planck-Institute for Polymer Research, Postfach 3148, D-55021 Mainz, Germany, and Institut für Makromolekulare Chemie, Universität Freiburg, Stefan-Meier-Str. 31, D-79104 Freiburg, Germany

Received August 8, 2002

ABSTRACT: We present solid-state NMR investigations of a series of shape-persistent polyphenylene dendrimers of generation 1−4 with different surface functionalization. Using a combination of traditional static and more advanced magic-angle spinning (MAS) exchange techniques for the elucidation of slow dynamics as well as fast-MAS recoupling techniques for the quantification of dynamic averaging in the megahertz range, we derive a clear picture of the complex molecular dynamics in these systems. Fast processes in the megahertz regime are shown to be restricted to fast vibrations of terminal phenyl rings with amplitudes of up to 40° at most, with a 5−30% fraction of rings performing larger-amplitude motions. Slow processes on the time scale of milliseconds to seconds are also restricted to terminal and doubly para-substituted phenyl rings. This type of motion is characterized by a two-site jump with a mean reorientation angle of 24° and a mean apparent activation energy of 34 kJ/mol and is presumably a concerted process involving several adjacent phenyl rings. The comparison of dendrimers with different surface functionalization allows us to conclude that the molecular dynamics are dominated by intramolecular steric constraints. As for the dependence on dendrimer generation, both the fast and the slow processes follow a trend that is expected from the evolution of the segment free volume at the periphery of the molecules, where most terminal rings are located. We therefore believe that our results represent the first experimental evidence of a class of dendrimers in which the radial segment density distribution is caused by truly extended arms and for which the dense-shell packing limit is reached for generation 4.

1. Introduction

The field of dendrimers, macromolecules with a regularly branched arm structure emanating from a well-defined focal point, is still enjoying an exponential increase in research activities.[1] Besides very promising applications of dendrimers as drug[2,3] and contrast agent carriers,[4] gene transfer agents,[5,6] or nanosized carrier in combinatorial synthesis,[7] the intriguing topological properties of these molecules have stimulated much theoretical[8−12] and experimental[13−23] work with respect to their particular molecular structure and dynamics both in solution and in the solid state. The focus of most of the work has been the elucidation of packing constraints, as imposed by the cascade topology, on the radial distribution and dynamics of segments located at different (topological) distances from the core.

While the first account of the synthetic realization of "cascade" or "starburst" growth by Vögtle and co-workers[24] went by almost unnoticed for several years, the work of Tomalia et al.[25,26] has actually provided the nucleus for rapidly increasing interest in these systems, which was mainly based on the possible rational design of molecular cavities providing mimics of biocatalytic sites or guest specificity. Such arguments were based on a rigid-shell model, assuming an exponentially increasing steric crowding of arms which should emanate radially from the core. Shortly after Maciejewski's first explicit mention of possible dense-shell guest inclusion,[27] and even before the first publication of Tomalia's synthetic breakthrough,[25] de Gennes and Hervet[8] established a self-consistent-field model of starburst growth. This work provided the basis for the dense-shell picture of dendrimers. While dendrimers may well be able to form cavities and accommodate molecular guests within the branched structure after attachment of a rigid shell of chemical different nature (a synonym of which has become renowned as Meijer's "dendritic box"[15]), the open core−dense shell notion put forth by de Gennes and Hervet was actually never verified, neither in any future theoretical nor in experimental work.

Computer simulations of increasing sophistication[9−11] and, finally, improved self-consistent-field arguments[12] consistently proved a density distribution with a maximum at, or close to, the central core. Boris and Rubinstein[12] explicitly mention the reason for the failure of de Gennes arguments: the increasing radial density is actually built into their model. Among the multitude of experimental work along these lines, Ballauff's recent results stand out in that, using SANS, it was finally possible to directly measure the structure factor associated with a decreasing radial density distribution.[17,23] The necessary back-folding of arms could directly be observed by solution-state NMR spectroscopy.[22]

So far, the majority of all work was devoted to dendrimers with arms made up of flexible units. However, dendrimers with rather *rigid* arms, incapable of considerable back-folding, may actually be expected to comply with the notion of increasing surface density of arms. Such dendrimers, solely built from phenylene units, were recently introduced by Miller et al.[28,29] and Müllen and co-workers.[30−32] Considerable rigidity and shape persistence of these molecules (Figure 1) were

* Corresponding authors. K.S.: phone +49-761-203-6310; fax +49-761-203-6306; e-mail kays@makro.uni-freiburg.de. H.W.S.: phone +49-6131-379-210; fax +49-6131-379-100; e-mail spiess@mpip-mainz.mpg.de.
[†] Max-Planck-Institute for Polymer Research.
[‡] Universität Freiburg.

10.1021/ma021283d CCC: $22.00
Published on Web 11/23/2002

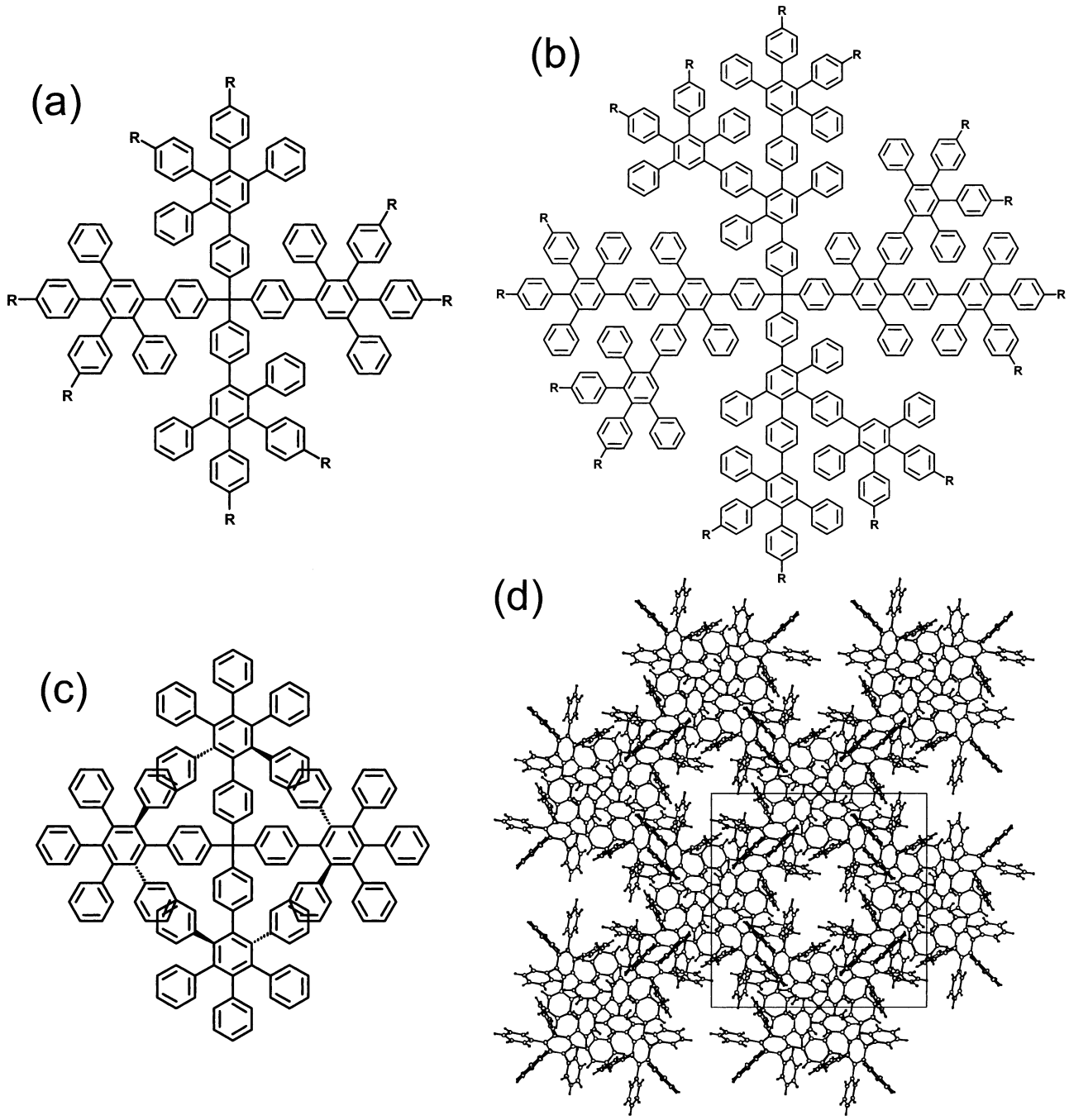

Figure 1. (a, b) Chemical structure of the differently functionalized, tetrahedral dendrimers of generation 1 and 2, respectively. R = −H, $-CH_3$, or $-C_{12}H_{25}$. (c) First-generation unsubstituted dendrimer $TdHexG_1H_8$, which exists in an amorphous and crystalline modification. (d) Projection of the corresponding crystal structure[54] with one elementary cell indicated.

proven by AFM[33] and molecular dynamics simulations.[30,34] In a forthcoming publication,[35] results from scattering will be reported which prove that, indeed, the density of molecular segments is larger at the surface of a dissolved polyphenylene dendrimer than in its center.

In a preliminary communication,[36] using solid-state NMR methods, we have correspondingly shown that molecular dynamics in these systems is rather limited. It was found that fast megahertz fluctuations of molecular units can occur only in a limited angular range, with only a very small fraction of units performing fast large-angle fluctuations. Independently, a slow process on the time scale of milliseconds to seconds was identified, and the counting statistics of the atoms performing this type of motion was shown to comply with reorientations being restricted to two-site jumps of terminal phenyl rings. Some uncertainty, however, remained on the exact geometry of this process.

Here, were give a detailed account of results from various static and magic-angle spinning (MAS) $^{13}C(-{}^{1}H)$ solid-state NMR experiments.[37] All of these experiments were applied to samples naturally abundant in ^{13}C, with no isotopic labeling necessary. We give details about the fraction of segments performing fast large-angle fluctuations and correlate these with temperature and molecular size. We as well report on the geometry and the time scale of the slow reorientation process of terminal phenyl rings as a function of temperature and dendrimer generation. Results from different types of

dendrimers varying in molecular geometry and functionalization are used to substantiate our conclusions. We discuss all our findings, also taking into account recent solid-state NMR investigations of flexible dendrimers.[18−21] The implications of our findings for rigid dendrimers of different generation will provide the basis of a revival of the original dense-shell picture for this particular kind of dendrimer.

The paper is structured as follows: the experimental part gives an overview of the various NMR methods used in this work and summarizes the type of information extractable from the different experiments. The first part of the results is devoted to the quantification of the fast dynamics, and in the second part, the restricted slow dynamics is elucidated. Both types of motions are discussed with respect to their temperature dependence and to possible influences of inter- or intramolecular packing. Finally, we discuss the interpretation of both types of dynamics with respect to their dependence on generation. Arguments are presented that are in accord with the notion that an increasing density of arms at the surface of these dendrimers indeed plays a role.

2. Experimental Section

Solid-state NMR experiments performed in this work can be subdivided in two classes. The first class is the represented by traditional two-dimensional (2D) *static* ^{13}C exchange NMR experiments,[37] used to elucidate the extent and geometry of slow reorientational processes. It is based on the classic three-pulse sequence, where the first pulse is replaced by cross-polarization (CP). Acquisition includes high-power ^{1}H CW dipolar decoupling (DD) after the third pulse and is preceded by a Hahn echo to eliminate dead-time problems. Figure 2a shows a representation of the pulse sequence.

All other experiments were conducted under MAS conditions, providing chemical selectivity for different types of functional groups in the molecule. The simplest MAS experiment is a one-pulse spectrum of ^{1}H under fast MAS conditions, where spectral resolution is already quite satisfactory when the spinning frequency exceeds 25 kHz and the B_0 field is sufficiently high.[38,39] This holds in particular for partly mobile systems, where simple analysis of the ^{1}H line width provides information about fast dynamic averaging of ^{1}H−^{1}H dipolar couplings, which are responsible for the line broadening.[40]

Another important source of information is the heteronuclear dipolar coupling between ^{13}C and ^{1}H. Anisotropic molecular motions in the megahertz range can be probed by their effect on the averaging of D_{CH} in molecular moieties with known rigid-limit coupling constants, such as CH, CH_2, or methyl groups. Under MAS conditions, 2D separated local-field spectra[41] provide the possibility of determining D_{CH} of spectrally resolved ^{13}C nuclei to their nearest ^{1}H neighbors under conditions of high ^{13}C resolution. This type of experiment gives precise results only when the ^{1}H nuclei are decoupled from each other in the indirect dimension, in which D_{CH} is probed. We used a simplified version in which the ^{1}H homodecoupling during t_1 is left to MAS alone, which was recently shown to be a robust and much simpler alternative[42] (see Figure 2b). Spinning sideband patterns in the indirect dimension of this experiment can be fitted to

$$S_{SLF} = \langle \prod_i \cos \Phi_{CH,i}(0,t_1) \rangle \qquad (1)$$

where the phase factor $\Phi_{CH,i}(0,t_1)$ depends on the dipolar tensor orientation and on the ratio between the coupling constant and the spinning frequency: $D_{CH,i}/\omega_R$. The product runs over all ^{1}H coupled to the detected ^{13}C and can be restricted to the dominating, directly bonded protons; angular brackets denote a powder average.

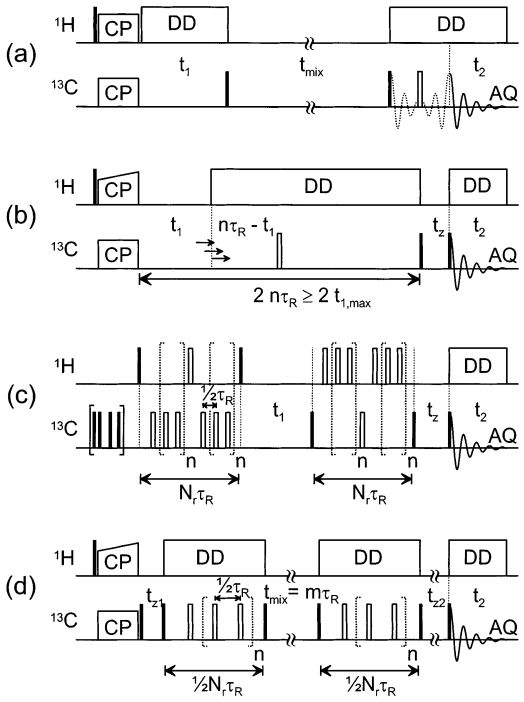

Figure 2. Pulse sequences of the solid-state NMR experiments used in this work. (a) Static ^{13}C exchange experiment featuring an initial cross-polarization and a Hahn echo before detection.[37] (b) ^{13}C($-^1$H) separated local-field (SLF) experiment performed under MAS conditions—^{1}H homodecoupling during t_1 is left to MAS alone.[42] (c) Recoupled polarization-transfer heteronuclear dipolar order rotor encoding (REPT-HDOR) experiment for the precision determination of ^{13}C−^{1}H dipolar coupling constants from spinning sidebands.[47] (d) Centerband-only detection of exchange experiment for the measurement of slow reorientational exchange processes under MAS.[49]

A second, also rather robust approach is based on the application of much higher MAS frequencies (25 kHz and more), at which ^{1}H homodecoupling by MAS is even more efficient, and D_{CH} can be determined quantitatively by way of reintroducing this coupling (which is also averaged out almost completely) by a recoupling sequence, which in our case is represented by a train of π pulses spaced by half a rotor period. This principle of recoupling, usually termed REDOR (rotational-echo, double-resonance), has become very popular for the determination of distances between pairs of heteronuclei.[43] Our sequence is efficient in that no initial CP is needed; ^{1}H polarization is used directly and transferred to ^{13}C in the course of the sequence.[44,45] We employ the principle of rotor encoding,[46] which leads to spinning sideband patterns in the indirect dimension of the 2D experiment, which is sensitively dependent on the magnitude of D_{CH}. The experiment is referred to as recoupled polarization-transfer heteronuclear dipolar order rotor encoding, REPT-HDOR.[47,48] The patterns are described by

$$S_{REPT} = \langle \sum_i \sin N_r \bar{\Phi}_{CH,i}(0) \sin N_r \bar{\Phi}_{CH,i}(t_1) \prod_{j \neq i} \cos N_r \bar{\Phi}_{CH,j}(t_1) \rangle \qquad (2)$$

where $\bar{\Phi}_{CH,i}(t)$ is the average phase factor associated with one of the two recoupling periods, which have a duration of N_r rotor periods each. See refs 47 and 48 for details on the notation; Figure 2c shows the pulse sequence. Most importantly, this experiment can be used in rather mobile systems, in which no spinning sideband information is apparent any more in a conventional MAS SLF experiment.

Recoupling by rotor-sychronized π pulses can also used for the ^{13}C chemical shift anisotropy (CSA). The CODEX (centerband-only detection of exchange) experiment[49] shown in Figure 2d is based on this principle; two identical rotor-synchronized

π-pulse trains of $N_r/2$ rotor periods length flank a mixing time, t_{mix}, during which the magnetization is stored along the B_0 direction. During t_{mix}, *slow* molecular reorientations may occur. The sequence is preceded by a cross-polarization. The application of the π-pulse trains leads to a stimulated echo at the end of the second train. The echo signal is given by

$$S_{codex} = \left\langle \cos \frac{N_r}{2}\bar{\Phi}_{csa,1} \cos \frac{N_r}{2}\bar{\Phi}_{csa,2} + \sin \frac{N_r}{2}\bar{\Phi}_{csa,1} \sin \frac{N_r}{2}\bar{\Phi}_{csa,2} \right\rangle \quad (3)$$

where $\bar{\Phi}_{csa,1}$ and $\bar{\Phi}_{csa,2}$ are again the integrated phases acquired during the first and second π-pulse train, respectively. A full echo signal $S_{codex} = 1$ is only obtained if $\bar{\Phi}_{csa,1} = \bar{\Phi}_{csa,2}$. Any change of $\bar{\Phi}_{csa}$, as induced by tensor reorientation during t_{mix}, leads to a characteristic signal loss, which can be used to extract the correlation time, t_c, of the motion. $\bar{\Phi}_{csa}$ depends on the CSA tensor orientation,[50] such that a variation of N_r at constant t_{mix} can be used to estimate the reorientation angle.

The plotted absolute exchange intensity

$$E(t_{mix}, N_r) = 1 - \frac{S_{codex}(t_{mix}, N_r)}{S_{codex}(t_{mix} = 0, N_r)} \quad (4)$$

obtained by normalization to an experiment with vanishing t_{mix}, approaches a plateau for long t_{mix} and N_r which depends on the number of molecular sites accessible to the dynamic process, M, and on the fraction of mobile segments, f_m:

$$E_\infty = f_m \frac{M-1}{M} \quad (5)$$

Most notably and opposed to static exchange spectroscopy, the CODEX method permits this type of analysis for any carbon site resolved in the ^{13}C CP MAS spectrum and is very sensitive to small rotation angles, for which exchange intensity in a static 2D spectrum would be very close to the diagonal and hard to detect.

To determine f_m and M unambiguously, the four-time CODEX experiment, which is fully described in ref 50, can be used. It basically consists of two consecutive CODEX sequences, the first of which serves to select the mobile fraction, while its exchange behavior is then probed by the second CODEX experiment. For reasons of referencing, four spectra have to be recorded, which differ only in the length of the mixing times, $t_{mix,1}$ and $t_{mix,2}$, of the two CODEX sequences. $1/M$ can be obtained independently of f_m according to

$$\frac{1}{M} = \frac{S_{4t}(0,\infty) - S_{4t}(t_{mix,1},\infty)}{S_{4t}(0;0) - S_{4t}(t_{mix,1},0)} \quad (6)$$

The two arguments of S_{4t} correspond to the two mixing times; the first mixing time $t_{mix,1}$ can, in principle, be chosen freely in two of the experiments, but for reasons of maximal signal it is usually chosen to be well in the plateau range, i.e., $t_{mix} \gg t_c$. The fraction of mobile segments f_m can subsequently be obtained from the regular CODEX plateau value E_∞.

The majority of the experiments were performed on a commercial Bruker DSX 300 spectrometer operating at a Larmor frequencies of 300.23 and 75.49 MHz for ^1H and ^{13}C, respectively. CODEX and SLF experiments were conducted with a 4 mm MAS double-resonance probe with zirconia rotors capable of spinning frequencies up to 15 kHz, while REPT-HDOR measurements necessitate faster spinning (25 kHz) and were performed with a 2.5 mm MAS double-resonance probe. Static exchange spectra were acquired on a double-tuned static Bruker probe with a 7 mm coil. Typical B_1 frequencies were 125 kHz (2.5 mm probes) and 83 kHz (4 mm MAS and static probes) for pulses on both channels and decoupling, while the power levels for CP, when applicable, were decreased. A ramp[51] was applied for CP under MAS. Fast-MAS ^1H spectra were obtained on a Bruker DRX 700 equipped with a 2.5 mm MAS probe. Frictional heating in all MAS probes was accounted for by suitable calibration procedures.[52]

Table 1. Dendrimers Investigated in This Work[a]

dendrimer	sum formula	molar mass [g/mol] calcd	molar mass [g/mol] exptl	no. of phenyl rings	ref
$TdG_1(CH_3)_8$	$C_{153}H_{116}$	1954.6	1954.7	24	36
$TdHexG_1H_8$	$C_{222}H_{150}$	2817.6	2816.4	28	31
$TdG_2(CH_3)_{16}$	$C_{401}H_{292}$	5133.7	5131.9	64	36
TdG_2H_{16}	$C_{385}H_{260}$	4886.3	4887.0	64	31
$TdG_2(C_{12}H_{25})_{16}$	$C_{577}H_{644}$	7618.7	7618.0	64	53
$TdG_3(CH_3)_{32}$	$C_{891}H_{640}$	11386.1	11414.9	144	36
TdG_3H_{32}	$C_{859}H_{580}$	10974.1	11006.0	144	31
TdG_4H_{64}	$C_{1825}H_{1220}$	23149.8	23217.0	304	31

[a] Td indicates that all dendrimers have a tetrahedral core with a functionality of 4.

Characteristics of the dendrimers investigated in this work are compiled in Table 1, and schematic representations of the dendrimers of generation 1 and 2 are shown in Figure 1a−c. The basic dendrimer structure consists of phenyl rings only, with the exception of a single aliphatic C at the center and different surface functionalization. All molecules are tetrahedral ("Td") in the sense that the core has a functionality of 4 (tetraphenylmethane); the branching coefficient for the arms is 2. The preparation of all dendrimers was reported in the literature[31,36] and in the PhD thesis of Wiesler.[53] The information on molecular weights in Table 1 demonstrates the high purity of the compounds and the efficiency of the divergent synthetic approach. All dendrimers are solid powders, and apart from a single sample (vide infra), DSC measurements show a flat line over the whole range from 100 K up to the decomposition temperatures of 500 and 800 K for substituted and unsubsituted dendrimers, respectively.[31]

The samples were used as-synthesized. Two samples stand out in that they have special physical properties. $TdHexG_1H_8$ has a very regular molecular shape and can be crystallized. Its X-ray structure is depicted in Figure 1d. The large voids are stabilized by solvent molecules.[54] When precipitated from solution, this dendrimer can also be obtained in an amorphous modification. Powder X-ray diffraction spectra of both modifications are shown below in the insets of Figure 8 and were obtained on a Siemens Kristalloflex 500 diffractometer using a Cu Kα radiation source and a graphite monochromator. Second, DSC traces of the alkyl-substituted $TdG_2(C_{12}H_{25})_{16}$ exhibit a weak solid to liquid-crystalline phase transition at around 240 K and a pronounced melting peak at 350 K. Lamellar (smectic) ordering with a layer spacing of 4.4 nm and characteristic birefringent textures were observed in this interval by powder X-ray diffraction and polarization microscopy, respectively.[53] This and other alkyl-substituted dendrimers were further shown to self-assemble on graphite surfaces to form two-dimensional crystals.[55]

3. Results

3.1. Fast Dynamics. 3.1.1. Fast Fraction. The first results on probing the rigidity of polyphenylene dendrimers by solid-state NMR were published in ref 36. Rigidity on a microsecond time scale was inferred from the measurement of the aromatic CH dipolar coupling constants by REPT-HDOR. Figure 3a shows a 2D spectrum, from which the spinning sideband patterns were extracted, which are shown in Figure 3b,c. In the high-resolution ^{13}C dimension, the signal of the tertiary aromatic CH groups is always roughly split in two, which correspond to CH groups in the ortho/para and meta position with respect to a quaternary ^{13}C bound to an adjacent phenyl ring. In none of the cases studied in this work did the separate analysis of these two signals yield any consistent additional information. Consequently, this group of signals, centered around 130 ppm, will always be treated as one.

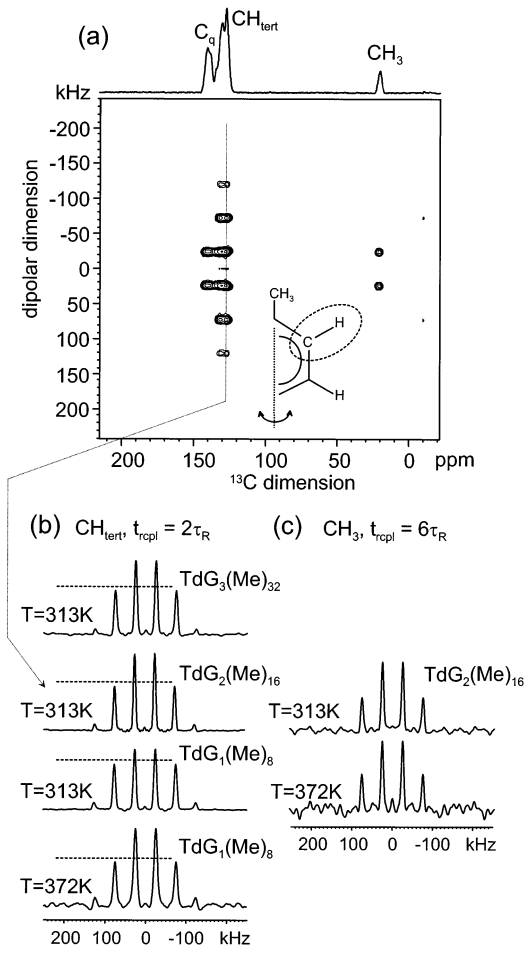

Figure 3. (a) Two-dimensional REPT-HDOR spectrum taken at ambient temperature (slight heating due to rotor friction) and 25 kHz MAS with $\tau_{rcpl} = 2\tau_R$. (b) Spinning sideband patterns, taken as slices along the dipolar dimension of spectra of different dendrimers and temperatures, extracted at the aromatic CH_{tert} signal positions. (c) Spinning sideband patterns of the CH_3 signal of $TdG_2(Me)_{16}$, acquired with $\tau_{rcpl} = 6\tau_R$. Dashed horizontal lines indicate the usual height of first-order sidebands in sideband patterns of rigid aromatic CH groups and permit the estimation of the amount of a fast fraction.

For the ensuing analysis, it is important to realize that signal for the quaternary aromatic carbons, C_q, is always shifted to the low-field end of the aromatic region and is well separated from signals due to CH_{tert}. The signal of C_q is not expected to overlap with CH_{tert}, first, because the signals were also found to be completely separated in solution-state *J*-modulated echo spectra and, second, because the spinning sideband patterns of CH_{tert} (slices along the dipolar dimension) are always identical across the whole range of signal for CH_{tert}. A contamination with C_q would lead to an increase of first-order sideband intensity at specific spectral positions and would very unlikely occur homogeneously throughout the 125−135 ppm range.

A quantitative analysis of the patterns in Figure 3b was presented in ref 36. In essence, the patterns can consistently be fitted to $D_{CH}/2\pi = 20.5$ kHz, corresponding to a rigid CH bond of 113 pm. Fast librational excursions up to about ±20° around para axes, however, would not influence this result much and could not be excluded. In fact, vibrations with a mean amplitude of 40° were also found in molecular dynamics simulations,[30,34] and the rather short proton T_1 relaxation time of $TdHexG_1H_8$ even in the crystalline modification (about 1 s, to be contrasted with tens of seconds for related rigid systems such as hexaphenylbenzene) gives additional confidence that such mobility is present. In the whole investigated temperature range of about 230−400 K, no onset of global, large-amplitude fast ring flips or whole arm reorientations, which would lead to a substantial decrease in spectral intensity and, upon increasing the correlation time further, to narrower CH patterns, was observed. This is in contrast to most other dendrimer systems with internal flexibility, which usually have a T_g and exhibit such phenomenology for $T > T_g$.

Interesting small and systematic deviations of the patterns from the theoretical prediction were, however, observed: while the consistent result for D_{CH} is obtained from fitting of the outer sidebands (ratio of fifth to third order sideband), the first-order sidebands exhibit a systematic deviation toward higher intensities. A small systematic deviation of that kind is generally observed for REPT-HDOR sideband patterns;[47] it is known to be due to long-range $^{13}C-^{1}H$ couplings and is influenced mainly by the local geometry (neighboring aromatic protons). The deviations observed here are, however, significantly bigger and were hypothesized to be due to a small fraction of rings that do perform larger amplitude motions with frequencies exceeding 100 kHz.

The deviation is shown in Figure 3b, where the dashed lines indicate the first-order sideband intensity which is usually observed in spectra of aromatic CH groups (the increase which is intrinsic to the experiment is included). The excess intensity is seen to increase with dendrimer generation from G_1 to G_2 and G_3, as well as temperature. Results of a systematic investigation are depicted in Figure 4, where the ratio of this intensity increase relative to the integral intensity of the whole pattern is plotted as a function of dendrimer generation (a) and temperature (b) and is denoted as "fast fraction". Note that the numbers thus determined do probably not reflect the number fraction of quickly mobile rings quantitatively, since relaxation/dephasing effects under the pulse sequence are probably different for two such populations with different mobility. The *systematic* variation of the value shown here is, however, well-suited for further interpretation.

The spinning sideband patterns for the terminal CH_3 groups in the methylated dendrimers, shown in Figure 3c, may help to elucidate the nature of this fast process. The patterns, which are obtained at longer recoupling times in order to make up for the reduced D_{CH} due to the fast methyl rotation, hardly change upon temperature variation. Methyl groups are always attached in the para position with respect to the core phenyl ring of every arm (see Figure 1) and are thus not influenced by motions around this axis. We therefore conclude that the fast fraction corresponds to quickly rotating/jumping terminal rings around the para axis. In our previous communication,[36] it was already shown that the process must involve *large-angle* jumps exceeding 90°; 180° is a probable candidate. The slow small-angle process to be discussed below, when being accelerated into the fast limit at higher temperatures, would not lead to a sufficient averaging of the CH dipolar coupling.

From Figure 4a, it is inferred that the fast fraction first increases upon going from the first to the second generation and then stays almost constant. This trend is only weakly dependent on the particular type of dendrimer (varying surface functionalization). This

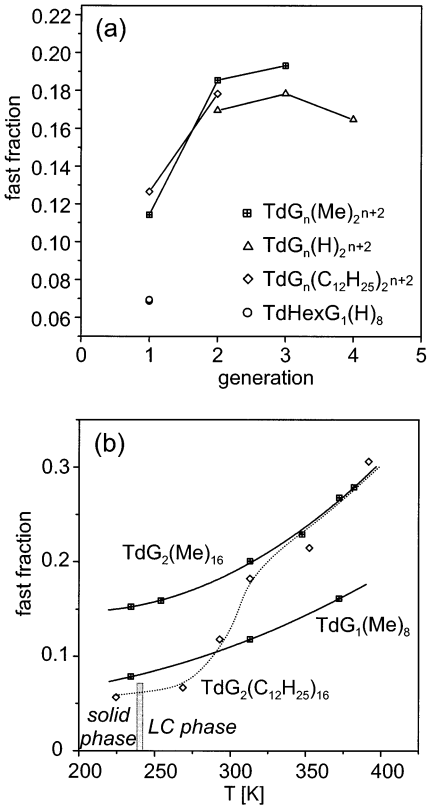

Figure 4. Fast fraction extracted from the REPT-HDOR spinning sideband patterns, plotted as a function of (a) dendrimer generation (T = 313 K) and (b) temperature. The lines are simply guides to the eye. The LC phase transition range for TdG$_2$(C$_{12}$H$_{25}$)$_{16}$ is also indicated in (b).

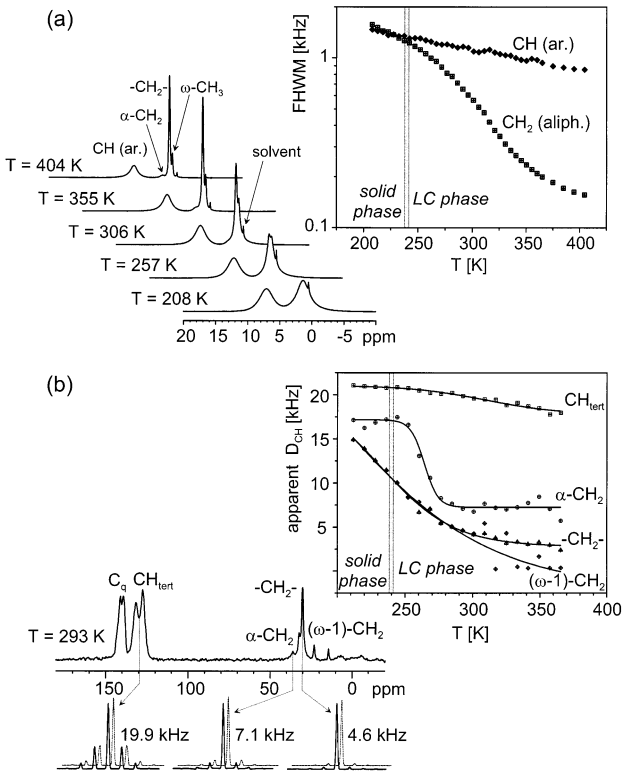

Figure 5. Fast-limit mobility in TdG$_2$(C$_{12}$H$_{25}$)$_{16}$ as investigated by (a) simple line-width analysis of ^{1}H MAS spectra (ν_R = 25 kHz) and (b) fitting of ^{13}C−^{1}H MAS SLF spinning sideband patterns (ν_R = 10 kHz). The plots in (a) and (b) show the full width at half-maximum (fwhm) of the ^{1}H line width and the heteronuclear dipolar coupling constant extracted from the MAS SLF patterns, respectively, for the indicated signal positions as a function of temperature. The fits in (b), plotted as dashed lines, were performed using the analytical solution for the signal of isolated and rigid CH or CH$_2$ moieties, where tetrahedral symmetry was assumed for the latter.

observation is most notable for the case of the dendrimer with long and, as shown below, pending mobile alkyl chains. Therefore, it is believed that the fast fraction is dominated by *intramolecular* steric constraints. This is corroborated by the low and identical values for amorphous and crystalline TdHexG$_1$Td, which has an additional terminal phenyl ring attached to the ring forming the center of every arm. This increases intramolecular steric crowding and inhibits fast flips.

For all dendrimers, the fast fraction increases with temperature, as shown in Figure 4b. This means that more and more rings attain motional frequencies in the fast-limit range. Here, the second-generation C$_{12}$H$_{25}$-substituted dendrimer stands out in that the fast fraction increases more strongly and in a sigmoidal fashion around 290 K. As will be shown below, this behavior must be associated with the onset of fast mobility in the presumably microphase-separated alkyl region between the polyphenylene scaffolds.

3.1.2. Dynamic Isolation of the Core. We now move to a more detailed investigation of the long-chain-substituted dendrimers, where microphase separation of rigid core and alkyl chain shell was hypothesized. The microphase separation is immediately proven by comparing simple ^{1}H MAS spectra at different temperatures (Figure 5a). At low temperatures, the spectrum consists of two homogeneously broadened lines in the ppm ranges for aliphatic chains and aromatic rings, and the line widths of roughly 2 ppm are of typical magnitude for rigid organic solids at 25 kHz MAS. Upon heating, considerable narrowing of the alkyl signals occurs, while the aromatic resonance hardly changes. This can be immediately associated with the onset of rapid chain motion and an averaging of dipolar couplings. The process can nicely be followed in the plot of the line width (full width at half-maximum, fwhm) vs the sample temperature (Figure 5a, right).

Despite a weak endothermic peak at 240 K, which was associated with a structural phase transition into a liquid-crystalline state,[53] DSC heating traces of the compound are rather featureless in the region of increasing alkyl motion, indicating a rather broad T_g of the chains. The structural phase transition occurs at much lower temperature than the onset of fast alkyl motion. Obviously, slow mobility of the alkyl chains, which allows for structural changes, sets in at even lower temperatures.

It is actually possible to prove that mobility sets in from the chain ends and that motional amplitudes decrease upon approaching the rigid core. This is achieved by quantitatively measuring CH dipolar coupling constants for the chain methylene groups, where the spectral resolution in a ^{13}C MAS spectrum is sufficient to differentiate signals from the chain end (ω-1 position), the main part of the chain, and the α-CH$_2$ at the core (Figure 5b). The method is very similar to the REPT technique shown above. Since REPT is not applicable to CH$_2$ groups,[47] we resorted to the simpler, but less quantitative, separated local-field method, which is explained in the Experimental Section.

CH dipolar coupling constants associated with the distinguishable methylene signals along the chain were

determined by fitting of sideband patterns which appear in the indirect dimension of such a 2D experiment. Sample patterns and fits are shown in Figure 5b. In the diagram, the so-obtained $D_{CH}/2\pi$ are compiled. The low-temperature limiting value of 17.4 kHz for the α-CH_2 is too low by about 4 kHz as a result of an interference effect of the strong ^1H homonuclear coupling within a CH_2 group, which is not supressed sufficiently well at the moderate spinning frequency used for this investigation. Faster spinning is not possible because the meaningful dipolar sidebands cannot be "pumped" by recoupling in in MAS SLF experiments and would vanish.

The method works better for the aromatic CH groups, where the correct result from the REPT investigations is reproduced at low temperature. In fact, the slight decrease of the value for $D_{CH}(CH_{tert})$ with temperature corresponds to the effect of the fast fraction as discussed above. The fast fraction leads to an increase of the *centerband* of MAS SLF sidebands, while the outer region is again found to be unchanged. The overall decrease in D_{CH} is only a consequence of the fact that the centerband was included in the fitting procedure for the MAS SLF sideband patterns.

The most prominent effect is observed for the α-CH_2, which exhibits a very narrow transition range into the fast limit and retains an almost constant D_{CH} up to high temperature. Clearly, this group merely performs rotations around the bond to the adjacent terminal phenyl ring. It is possible to give a quantitative interpretation in terms of a local dynamic order parameter

$$S_{CH} = \left| \frac{D_{CH,dyn}}{\frac{1}{2}(3\cos^2\alpha - 1)D_{CH,stat}} \right| \qquad (7)$$

where α is the angle of the two CH bond vectors with respect to the rotation axis, which coincides with the CC bond to the phenyl ring. Therefore, α = 109.5°. $S_{CH} = 0.98 \pm 0.08$ proves the stability of the rotation axis. This value is obtained only when a realistic $D_{CH,stat}$ of 21 kHz is used. As discussed, the low-temperature value of 17 kHz from the same series of experiments is subject to a large systematic error. The error is much smaller for $D_{CH,dyn}$ of the rotating CH_2 group due to an efficient self-decoupling of perturbing HH interactions as a result of the rotation.

We have thus proven that the alkyl chains are attached to a rigid object. The chain end starts to move much earlier than the α-CH_2, and averaging over wider angular ranges persists in the whole range of measurement.

3.2. Slow Dynamics. 3.2.1. 2D Static ^{13}C Exchange Spectroscopy. Our next concern will be the study of *slow* motions in the milliseconds to seconds range, which show no effect in the dipolar experiments discussed so far. Static 2D ^{13}C exchange spectroscopy is a well-established method to study such slow processes.[37] Therefore, static 2D exchange spectra were acquired for all dendrimers in our series and provide preliminary insight into slow motions in the dendrimers. Figure 6 shows two representative spectra of amorphous $TdHexG_1H_8$ taken at 100 °C at two different mixing times. The most notable observation is the *absence* of considerable off-diagonal exchange intensity. Even after 4 s, most of the intensity is still concentrated on the diagonal. This lets us conclude that no large-scale

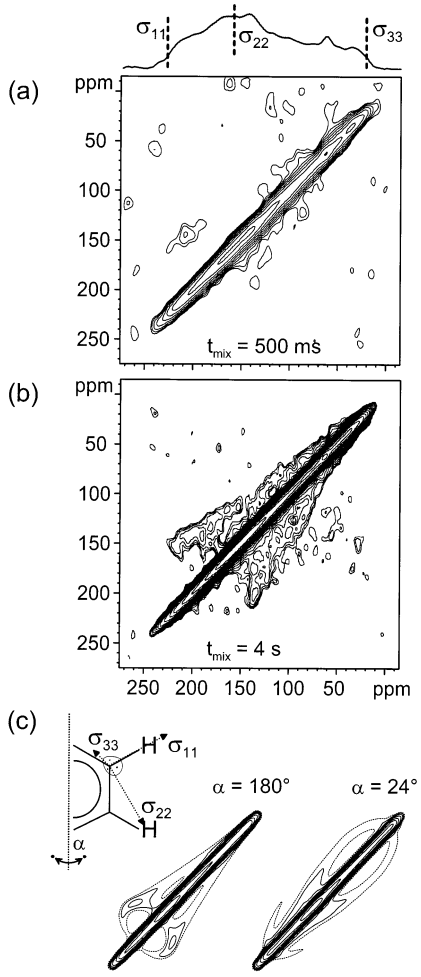

Figure 6. Slow molecular reorientations in amorphous $TdHexG_1H_8$ as investigated by static ^{13}C exchange spectroscopy. (a) and (b) show experimental spectra taken at 373 K with mixing times indicated. The contour lines are logarithmic (increment factor 1.5) and start at about 3% of the maximum intensity. (c) Numerical simulations of exchange spectra of the same dendrimer based on the motional models discussed in section 3.2.3. Contour levels are logarithmic, matching the ones in the experimental spectra. The dashed lines in (a) indicate the approximate spectral positions of the three CSA principal values.

reorientations of whole dendrimer arms or arm segments occur in the range of seconds.

In the spectrum in Figure 6b, the exchange intensity close to the diagonal is apparent above the noise, but its intensity does not exceed 10% of the integral intensity (the contours are logarithmic). Even though the appearance of this off-diagonal intensity might be taken as an indication of the presence of slow and very restricted motional processes, which is indeed found, we will later see that the off-diagonal intensity in Figure 6b is in fact dominated by slow $^{13}C-^{13}C$ spin diffusion. We will return to the implications arising from the static 2D exchange data when discussing the motional model derived from the data of the 1D MAS exchange experiments.

3.2.2. Correlation Times. Static 2D exchange spectroscopy, in particular when performed in natural abundance, is not well-suited to study correlation times in detail—the acquisition of each of the spectra in Figure 6 took about 2 days! The CODEX experiment, a 1D exchange method with high ^{13}C resolution, fills this gap. As detailed in the Experimental Section, with this

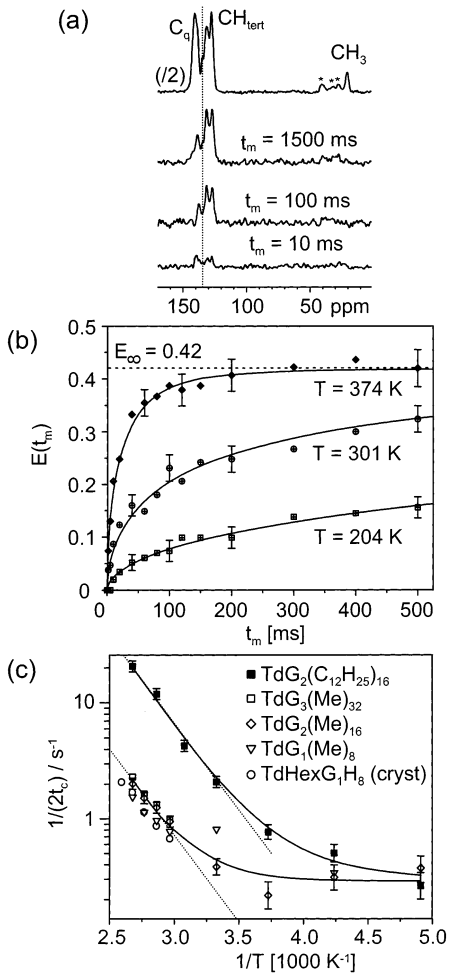

Figure 7. Data from CODEX experiments for the determination of slow-motional correlation times. (a) Experimental CODEX spectra for TdG_2Me_{16} measured at 349 K, 7.5 kHz MAS, and a recoupling time of 0.8 ms (six rotor periods). Mixing times are indicated at the spectra; the top spectrum is the reference spectrum. Asterisks denote spinning sidebands. (b) CODEX exchange intensities corresponding to the averaged intensities of the CH_{tert} as a function of the mixing time for three different temperatures. The correlation functions plotted as solid lines are based on KWW fits. (c) Arrhenius plot of the correlation rates ($= {}^1/_2 t_c$ in the case of a two-site jump) for the various dendrimers. Solid lines are fits to a function which includes a temperature-independent contribution from spin diffusion (see text), and dotted lines indicate the trends for absent spin diffusion.

technique it is possible to study correlation times and rotation angles in a site-resolved fashion by simple variation of the mixing time and the recoupling time, respectively. In ref 36, we have already shown that slow motions with a distribution of correlation times are present, that they are restricted to reorientations of terminal rings, and that they must be different from the commonly observed 180° flip. We will recapitulate these findings upon presenting an in-depth treatment including the determination of activation energies and the elucidation of the exact geometry of the process.

Typical CODEX exchange spectra are shown in Figure 7a. While the reference spectrum on top is almost identical to the regular MAS spectrum, the pure-exchange spectra below show only signals from molecular fragments which must have reoriented during t_{mix}. The existence of nonzero exchange intensity for the C_q is actually the proof that the process cannot be modeled by a 180° flip—such a process would be symmetry conserving for all quaternary carbon CSA tensors and not lead to any signal. We will return to geometry considerations later and first discuss the correlation times, which were determined from the t_{mix} dependence of the exchange intensity of the CH_{tert} signals, as plotted in Figure 7b.

Table 2. E_∞ As Determined as the Average over Double-Exponential Fits to Correlation Functions Measured at $T > 340$ K (Mean Error: ±0.04) and Theoretical Values for Two Different Models Including Non-180° Two-Site Jumps of Terminal (Model 1) or All (Model 2) Para-Substituted Phenyl Rings[a]

		model 1		model 2	
dendrimer	exptl CH_{tert}	CH_{tert}	(C_q)	CH_{tert}	(C_q)
$TdG_1(CH_3)_8$	0.362	0.39	(0.21)	0.48	(0.29)
$TdHexG_1H_8$	0.419 (am), 0.395 (cryst)	0.43	(0.19)	0.5	(0.27)
TdG_2R_{16}	0.428 (R = CH_3), 0.430 (R = $C_{12}H_{25}$)	0.30	(0.18)	0.48	(0.27)
TdG_2H_{16}	0.410	0.31	(0.14)	0.48	(0.24)
$TdG_3(CH_3)_{32}$	0.421	0.26	(0.16)	0.47	(0.27)
TdG_3H_{32}	0.440	0.28	(0.11)	0.48	(0.25)
TdG_4H_{64}	0.440	0.25	(0.11)	0.48	(0.25)

[a] Experimental values for C_q could not be extrapolated by fitting but were always in the range of 0.1−0.2 at the longest T_{mix}.

The correlation functions were found to be non-exponential. A KWW expression ($E(t) = E_\infty(1 - \exp\{-(t_{mix}/t_c)^\beta\})$) provided good fits in all cases, and the average β was 0.51 ± 0.05, indicating a distribution of correlation times of about 2 orders of magnitude. The distribution leads to a problem concerning the determination of the long-time plateau intensity E_∞, which contains valuable information on the number of sites accessible to the process. As data for sufficiently long t_{mix} are already significantly influenced by $^{13}C-^{13}C$ spin diffusion (vide infra), the KWW fit did not provide a stable fit for E_∞ (spin diffusion is a multisite process, which ultimately leads to $E_\infty = 1$).

As a resort, all data from temperatures above 340 K and mixing times up to 2 s were fitted to a double-exponential function, which permitted a consistent determination the plateau value. The fixed average plateau values for the higher temperatures (collected in Table 2) were then used for the KWW fits of the whole temperature series. Note that exchange intensities associated with C_q are roughly compatible with the results thus obtained. However, since the considerably lower value of E_∞ associated with this signal leads to a much stronger *relative* influence of spin diffusion effects on the data, C_q exchange intensities were not attempted to be analyzed quantitatively.

The inverse t_c thus determined are shown in an Arrhenius plot (Figure 7c). The factor of 2 in $k = 1/(2t_c)$ takes into account that the process is a two-site jump, to be proven below. Most notably, the data seem to approach a constant value at low temperatures. This phenomenology is a clear fingerprint of temperature-independent $^{13}C-^{13}C$ spin diffusion. It can be accounted for by fitting ln k in an Arrhenius plot by[56]

$$\ln k = \ln(k_0 e^{-E_a/kT} + k_{sd}) \qquad (8)$$

where k_{sd} is the spin diffusion rate. This simple fitting function is purely heuristic. The assumption that the two rates are additive implies that the geometry (thus the associated E_∞ values in CODEX) of the two processes is the same, which need not be the case (additivity of

rates implies the observation of a singly exponential correlation function!). Therefore, results for k_0 and E_a must be interpreted with care. Within experimental accuracy, k_{sd} was the same for all dendrimers and amounted to 0.31 ± 0.06 s^{-1}, which is a surprisingly high value. A detailed discussion of such a high $^{13}C-^{13}C$ spin diffusion rate in a naturally abundant sample is beyond the scope of his paper. We may just mention that rates of similar magnitude were also observed between aromatic carbons in crystalline durene (1,2,4,5-tetramethylbenzene),[57] which, just like the investigated dendrimers, is an aromatic molecule with terminal methyl groups. More commonly, rates of this magnitude (and higher) are observed only in ^{13}C-enriched systems.[58]

Since spin diffusion is seen to exert its adverse effect mainly on low-temperature data, and the value of β did not change significantly even at high temperature, we conclude that the distribution of correlation times is intrinsic to the process and not an artifact caused by spin diffusion. The intrinsic distribution of t_c explains why the two correlation times from double-exponential fits are not interpretable in a consistent way.

The average values for E_a and k_0 for the methylated dendrimers of generation 1−3 are 36 ± 10 kJ/mol and $(1.9 \pm 2.4) \times 10^6$ s^{-1}, respectively, while $TdG_2(C_{12}H_{25})_{16}$ has $E_a = 31 \pm 4$ kJ/mol and $k_0 = (3.3 \pm 2.5) \times 10^6$ s^{-1}. Obviously, the frequency factors are ill-defined as a result of the limited temperature range. Values of up to 10^{-9} s^{-1} can still be reconciled with the data, which is much lower than values of $10^{-14}-10^{-15}$ s^{-1} expected for an elementary jump process. Lower values are, however, commonly found for phenyl reorientations (π flips in most cases) in complex polymer systems like poly(ethylene terephthalate) ($E_a = 42$ kJ/mol, $k_0 \approx 4 \times 10^6$ s^{-1} (ref 59)) or polycarbonate ($E_a = 37$ kJ/mol, $k_0 \approx 10^{13}$ s^{-1} (ref 60)), where low frequency factors are usually discussed in terms of the complexity and cooperativity of the dynamic process. The reconciliation of an empirical KWW fit (to account for an apparent distribution) with an Arrhenius-type analysis (implying an elementary process leading to exponential relaxation) is always problematic. We also favor an interpretation of the jump motion in the dendrimer as being cooperative, and we will come back to this issue in the Discussion section.

The values for E_a of methyl- and alkyl-substituted dendrimers are identical within experimental error, which is surprising in view of the up to 10 times higher correlation rates for the chain-substituted dendrimer. Just like for the "fast fraction" identified in section 3.1, the alkyl matrix does not seem to substantially influence the microscopic intracore nature of the slow process (as characterized by E_a), but more subtle effects on correlation rates or a quick increase in the fast fraction (Figure 4b) are clearly present. Unfortunately, an investigation of the effect of alkyl matrix solidification on the slow process is not possible because slow exchange correlation times in the temperature range where the alkyl chains are frozen are not accessible due to the spin diffusion problem.

A further confirmation of the weak effect of intermolecular packing on the correlation time of the slow process comes from a comparison of t_c for the crystalline and the amorphous modification of $TdHexG_1H_8$, shown in Figure 8. The rates are very similar, yet somewhat lower, for the crystalline modification. This is surprising,

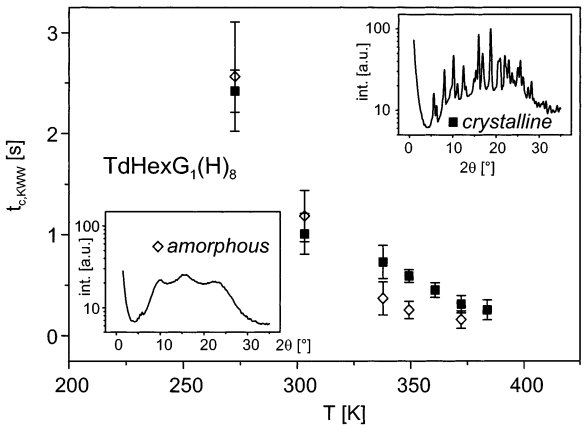

Figure 8. Comparison of the correlation times for the two modifications of $TdHexG_1H_8$ as a function of temperature. The insets show powder X-ray diffraction intensities as a function of the scattering angle, θ.

since the crystals are known to exhibit large solvent-filled voids and lack considerable intermolecular arm interdigitation (see Figure 1d). The crystals decompose into the amorphous modification upon heating and loss of solvent,[54] which might imply denser packing and lower rates for the latter. The assumption that intramolecular constraints are dominant can better explain lower rates for a crystal, where steric constraints posed by neighboring arms cannot be relaxed as easily as in an amorphous packing environment. We take the finding of faster dynamics for the amorphous modification as a valuable hint that arm interdigitation does not play a significant role in the global dynamics of the dendrimers.

In summary, we repeat the preliminary conclusion that we have identified and quantified a slow motional process restricted to *local* reorientations of terminal phenyl rings, the exact geometry of which is to be determined in the next section. The interpretation of the weak but significant generation dependence of t_c, as apparent from Figure 7c, will be further deferred to the Discussion section.

3.2.3. Geometry of Motion. The number of sites accessible to the slow process is encoded in the long-time plateau E_∞ of the exchange intensity. The plateau values, as determined from fits to the high-temperature correlation functions, are listed in Table 2. The spin diffusion problem is the most serious source of error for these values; therefore, they might be somewhat *overestimated*. The values for CH_{tert} are consistently lower than 0.5, which excludes any multisite process involving most C atoms in the dendrimers. Since the plateau for an M-site jump is $(M - 1)/M \geq 0.5$, there must be a fraction of atoms that are either immobile or have a CSA tensor which is invariant under the process.

We have already seen that the existence of nonzero exchange intensity for the C_q signals rules out exclusive 180° flips around the para axes, which would represent the most probable candidate for a simple two-site jump. However, assuming two-site jumps with a different angle, we can calculate possible plateau values for all generations, which comply with the observations, by simple counting statistics. This involves counting all aromatic carbon atoms of a particular dendrimer, determining how many carbons belong to rings which are assumed to be mobile, and calculating E_∞ according to eq 5. A comparison of experimental values with calculated ones can be taken from Table 2. Experimental

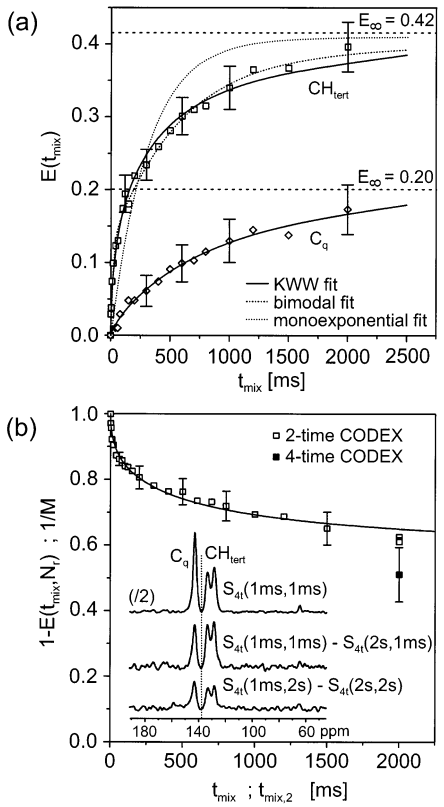

Figure 9. (a) CODEX data for the tertiary CH and quaternary C signals of TdG_2Me_{16} at 349 K (see also Figure 7) with plateau values indicated by dashed lines. (b) Comparison of 2-time and 4-time CODEX intensities measured for the tertiary CH signals of amorphous $TdHexG_1H_8$ at 337 K, 7.5 kHz MAS, and 6 τ_R recoupling. The conventional 2-time CODEX data are plotted as *dephasing*, i.e., $1 - E(t_{mix}) = S(t_{mix})/S(t_{mix} = 0)$. The mixing times for the 4-time CODEX experiments are shown above the corresponding spectra in the inset.

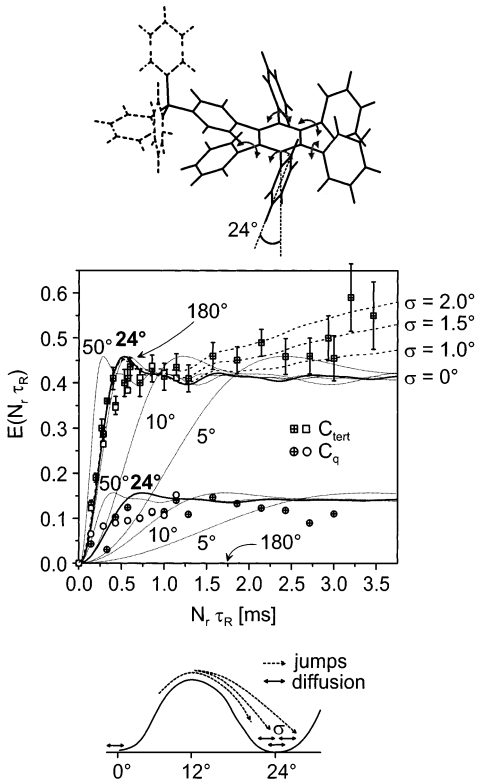

Figure 10. Determination of the geometry of slow motions from the recoupling time dependence of CODEX intensities for $TdG_2(Me)_{16}$ (crossed symbols) and crystalline $TdHexG_1H_8$ (open symbols), measured at 14 kHz MAS and $T = 361$ K, $t_{mix} = 1.5$ s for the former, and $T = 374$ K, $t_{mix} = 0.8$ s for the latter. The plot includes model curves calculated for various reorientation angles. Corresponding models are also depicted.

values are found to lie between the values predicted from a model where only terminal rings perform jumps (model 1) and another model, where all doubly para-substituted rings in the interior of the molecule are included in the jump motion (model 2).

Experimental exchange intensities for C_q at long t_{mix} were always found to be in the range of 0.1−0.2. As an example, Figure 9a shows buildup data for C_q in comparison with CH_{tert}. Note that the indicated KWW fit merely represents a guide to the eye, since the associated E_∞ was not determined in a consistent way. Such values would favor model 1, where only terminal rings perform small-angle jumps. When *inner rings* are hypothesized to perform 180° flips (which leaves the associated C_q intensities unchanged), E_∞ of *all* C_q would be given by model 1, while model 2 would apply for E_∞ of CH_{tert}. This assumption would explain our experimental data best, in particular considering that spin diffusion effects lead to an overestimation of experimental values. However, considering the large error associated with all experimental values for E_∞, we hesitate to present this as a definite conclusion.

Our motional models presented so far rest on the assumption of a two-site jump. Apart from being justified by the rather low value for E_∞, the number of sites M can be assessed quantitatively from the (very time-consuming) 4-time CODEX experiment. The experiment was performed on amorphous $TdHexG_1H_8$; spectra and the result are shown in Figure 9b, where the single point from the 4-time CODEX experiment, $1/M = 0.49 \pm 0.08$, is compared with the regular 2-time *dephasing* curve. First, the result is consistent with $M = 2$. $M = 3$ would lead to a result of 0.33, which is well outside the range of the error limits. Second, the difference between $1/M = 0.5$ and the 2-time CODEX dephasing directly represents the fraction of immobile sites, which, in the framework of our motional model, is related to CH_{tert} positions on rings that do not participate in the motion.

For the quaternary sites, we determine $1/M = 0.62 \pm 0.08$, which is slightly larger and *unphysical*. The result being larger than 0.5 confirms that the process involves two sites at most, while the deviation toward unphysical values gives confidence that spin diffusion did not distort the 4-time CODEX result considerably: spin diffusion is intrinsically a multisite process and can only be held responsible for decreasing (instead of increasing) the result for $1/M$. The error is more likely due to an underestimation of experimental noise or to the finite value of $t_{mix,2} = 2$ s, which is not sufficient to reach detailed balance. The mean correlation time as determined from the KWW fit was 530 ms at 337 K, so the correlation time distribution leads to a contribution from sites that do not reorient within 2 s, which in turn increases the apparent $1/M$.

Recoupling-time-dependent CODEX curves were used to elucidate the geometry of the reorientation process further. Results for crystalline $TdHexG_1H_8$ and $TdG_2(CH_3)_{16}$ are plotted together in Figure 10. Their close coincidence proves that the geometry of the processes is determined by intramolecular packing and is hardly dependent on the existence of the additional phenyl ring in each arm of $TdHexG_1H_8$ (see Figure 1). In addition,

Table 3. CSA Principal Values Determined by the SUPER Experiment[61] Performed on Amorphous TdHexG$_1$H$_8$[a]

	ppm			kHz		
	σ_{11}	σ_{22}	σ_{33}	σ_{11}	σ_{22}	σ_{33}
CH_{tert}	227	147	16	17.1	11.1	1.2
C_q	240	163	21	18.1	12.3	1.6

[a] Values in kHz correspond to $\omega_L^C/2\pi = 75.5$ MHz. For experimental details see ref 62. Values for CH_{tert} are averaged over the two positions, assuming a common σ_{iso} of 130 ppm. The mean errors are ±4 ppm and ±0.3 kHz, respectively.

corresponding data (not shown) taken at a mixing time of 150 ms exhibit the same trend, with the only difference to the long-t_{mix} data being an expected decrease in the plateau value. This proves that the faster population in the correlation time distribution does not exhibit a significantly different angular characteristic than the slower population.

Theoretical curves were calculated from eq 3 for different rotation angles around the para axis; the assumed geometry is depicted to the left of the plot and in Figure 6c. Principal values for the CSA tensors (see Table 3) were determined using the SUPER (separation of undistorted powder patterns by effortless recoupling) technique,[61] which is a very powerful and robust MAS recoupling method permitting a straightforward 2D correlation of the high-resolution isotropic shift with the associated quasi-static powder pattern. The experimental details for this study can be taken from ref 62. The assignment to molecular axes as shown in Figure 6c is based on literature data of CSA principal values and directions in a variety of aromatic compounds.[63] The curves for CH_{tert} and C_q were calculated assuming ortho/meta positions and auto/para positions, respectively, with respect to the rotation axis. The 12−20% CH_{tert} groups located on the rotation axis were neglected.

The experimental exchange intensities for CH_{tert} in Figure 10 can equally well be described assuming rotation angles around the para axis of 24° and 180°. This ambiguity arises from the 60° relative orientation of the σ_{11} principal value direction of the asymmetric CSA tensor with respect to the rotation axis (see Figure 6c), leading to the quickest initial rise in exchange signal for 90° jumps. Note that the curve for 180°−24° is *not* identical to the one for 24°, as would be the case for an axially symmetric CSA tensor. As already mentioned, the mere existence of nonzero exchange intensity for C_q at rather short recoupling times excludes reorientations close to 180° as the main contributor. As hypothesized above, it is possible that some doubly para-substituted rings located more to the center of the molecules perform 180° flips.

The majority of *terminal* rings, however, apparently undergo two-site jumps with a mean rotation angle of 24 ± 3°. The different value of 60° given in ref 36 was based on preliminary estimations and a crude comparison with the crystal structure, where a tilt of 30° of each terminal ring relative to the normal of the central ring plane, to which it is attached, suggested a local symmetry-conserving 60° jump. The exact average tilt angle was later found to be 26°.[54] We will return to a more detailed interpretation in section 3.3.1.

The value of 24° does not change even when the simultaneous presence of fast librations with up to 40° amplitudes, as discussed in section 3.1, is considered. Apart from the weak partial averaging of the CSA and heteronuclear dipolar tensors (which reduces δ by less than 20% and is thus hardly measurable), such motions change the tilt angle of the σ_{11} direction with respect to the para axis from 60° to 53°, which, however, has no significant influence on the CODEX build-up curves shown in Figure 10.

Also, the characteristic first maximum of the theoretical curve is not fully reproduced experimentally. Such phenomenology has been observed in other studies[62,64] and can be explained by changes of CSA principal values upon reorientation or by a small distribution of jump angles. Changes of CSA principal values can be caused by their dependence on the relative orientation of two directly bonded phenyl rings[65] and by changes in $\pi-\pi$ packing ("ring current effects") induced by neighboring phenyl rings,[66] which both change for non-180° flips.

At long recoupling times, an increase of $E(N_r\tau R)$ over the plateau value of 0.42 is apparent. This behavior is also typical for a small distribution of jump angles (for subsequent jumps of the *same* nucleus) or slow small-angle diffusive motions.[64,67] Both processes lead to an increase in $E(N_r\tau R)$ at long $N_r\tau R$, where CODEX becomes sensitive to very small rotation angles[50] or, as is the case here, small differences in successive rotation angles due to imprecision of the return jumps. Such a scenario can be explained in terms of a shallow potential minimum around the mean reorientation angle, as indicated at the bottom of Figure 10, and also gives a straightforward rationale for the observed distribution of correlation times.[67]

Finally, the consistency between our motional model as derived from the 1D MAS exchange studies and the 2D static exchange data presented in Figure 6 needs to be checked. Therefore, we have calculated static 2D exchange spectra based on the CSA tensor values from Table 3, assuming full exchange as described by the counting statistics for TdHexG$_1$H$_8$ according to model 1 (reorientations of terminal rings only, see Table 2). Simulations for $\alpha = 24°$ and $\alpha = 180°$ are compared to the experimental spectra in Figure 6, where care has been taken to match both the line widths and the lowest contour levels (shown as dashed lines in the simulations).

At 373 K, the mean correlation time of TdHexG$_1$H$_8$ as measured by CODEX is approximately 200 ms. Therefore, the spectrum in Figure 6a should be close to full exchange. No significant exchange intensity is apparent above the noise level, and the comparison with (c) confirms that this can also not be expected considering the given S/N, also keeping in mind that (i) $t_{mix} = 500$ ms is not sufficient to reach full exchange in particular for segments located at the slower end of the correlation time distribution and (ii) a distribution jump angles around 24° would blur the characteristic exchange pattern even further. Therefore, the exchange intensity observed at $t_{mix} = 4$ s must be attributed to spin exchange.

The similarity of the 4 s exchange spectrum to the signature of 180° flips shown in Figure 6c can be interpreted as an indication of a preferential exchange of polarization between carbons that share a common direction of the σ_{33} axes (i.e., the ring normal), which means that intra-ring transfer or transfer between carbons in coplanar rings is preferred. Note that, even though the interpretation of the exchange pattern in (b) in terms of π flips of inner phenylene rings might represent an appealing option, it can be excluded because such a process would not lead to the observed

intensity. We close in stating again that, in contrast to the weak effect of the slow process in static 2D exchange spectra, the CODEX technique proved to be very suitable for the detection and quantification of the restricted molecular dynamics in polyphenylene dendrimers, particularly because of its ability to detect small-angle tensor reorientations[50] or small fractions of mobile sites (C_q in our case).

3.3. Discussion. We have found two characteristic regimes of molecular mobility in the polyphenylene dendrimers, which pertain only to terminal or doubly para-substituted phenyl rings: (i) fast motions in the megahertz range, which lead to fast T_1 relaxation of protons (even in a crystalline modification) and partial motional averaging of heteronuclear dipolar interactions, and (ii) slow motions in the seconds to milliseconds range, which were probed by reorientations of CSA tensors associated with aromatic carbon atoms. Slow or fast large-amplitude motions of whole arm segments can definitely be excluded for temperatures up to 400 K. In particular, we have identified (1) fast librational motions whose amplitude could be as high as 40°, (2) a small fraction (5−30% of the integral signal) of rings performing fast large-amplitude flips or rotations, which increases with generation and temperature, and (3) slow two-site jumps with a mean reorientation angle of 24° around the para axes, which exhibit an apparent activation energy of 33 kJ/mol and correlation times which increase with dendrimer generation and exhibit a constant distribution over about 2 orders of magnitude as the dominating motional processes. Both fast and slow processes were found to be mostly dependent upon *intramolecular* steric constraints. Owing to the rigidity of the dendrimer scaffold, the majority of terminal phenyl rings are located close to the periphery of the molecules, indicating that the generation dependencies can provide information on segment packing at the periphery.

3.3.1. Correlation Time Distribution and Molecular Model. We first turn to motivate the plausibility of the appearance of two motional regimes and the molecular origin of the slow two-site jump. In Figure 11, two scenarios for the possible observation of two dynamic regimes are compared. We might assume a very broad distribution of correlation times extending from the fast limit to very slow exchange (a) or two narrower separate distributions (b). Several arguments can be given which are in disagreement with a monomodal model:

(i) The mean jump angle of the dominating slow process is too low to explain an exclusive increase of first-order sidebands in REPT spectra when a tail of the process is assumed to reach the fast limit.[36]

(ii) Upon application of recoupling pulse sequences, a large amount of spectral intensity is lost when the correlation time of a process enters the intermediate motional regime.[68] Apart from an intensity decrease due to the usual Curie factor ($\sim\hbar\omega_L/kT$), however, such a pronounced intensity loss was not observed at higher temperatures.

(iii) The normalized plateau value in CODEX is also expected to decrease significantly when intermediate motions are present.[68] Within experimental accuracy, a reduction of the plateau was not observed, indicating that the correlation time distribution of the slow process does not significantly extend into the milliseconds range.

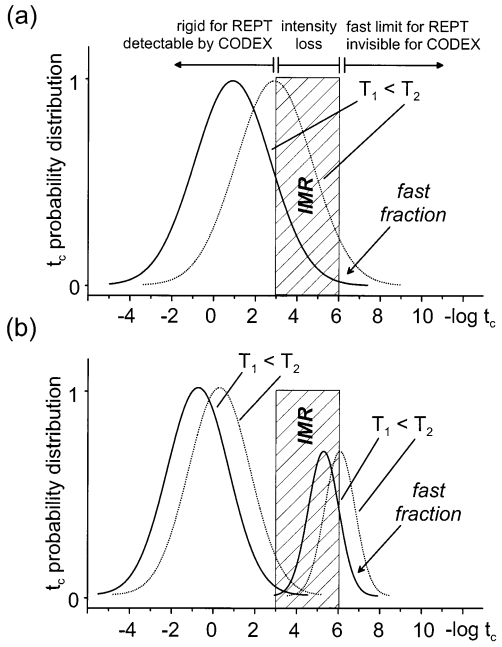

Figure 11. Effect of broad mono- (a) and bimodal (b) correlation time distributions on the spectral intensity observed in the different recoupling experiments. The intermediate motional regime (IMR) is characterized by substantial signal loss over a wide range of correlation times.

(iv) Accordingly, the stretch exponent β from the KWW fit did not change with temperature, which would be the case when parts of the correlation time distribution would become invisible to the experiment.

We therefore favor the notion according to which the fast fraction is a separate process (Figure 11b), the mean correlation time of which shifts away from the intermediate motional regime with increasing temperature within the experimentally accessible range, leading to the observed increase of the fast fraction with increasing temperature.

To discuss the molecular origin of these processes in the dendrimer, we report the recent results of a solid-state ^{2}H NMR study of phenyl ring dynamics in crystalline *o*-terphenyl (benzene with two phenyl substituents in the ortho position) by Haeberlen et al.[69] The seemingly equivalent terminal phenyl rings in this compound are in fact crystallographically *inequivalent*, allowing for spectral differentiation in a single-crystal study. The two rings were found to undergo 180° flips with exponential correlation functions and correlation times differing by 2 orders of magnitude! For eample, room temperature rates are approximately 0.03 and 30 Hz, respectively. The activation energies for the two rings were found to be *identical* (80.5 ± 3 kJ/mol) within very small error limits. The difference arises from the apparent preexponential factors k_0. The molecular origin of this rather counterintuitive behavior still remains unclear. Haeberlen gives a cautionary interpretation in terms of fast flips of one ring pushing the neighboring one and causing a flip of the latter only with very low probability. This probability will also depend on of the local packing environment. Such a probabilistic statement entails that the flips are *not* strictly correlated, i.e., that the flips do not occur concertedly, yet they may be interdependent.

Turning to the polyphenylene dendrimer case, we identify the same local pattern of mutual steric hindrance of phenyl rings as in *o*-terphenyl, with even

higher steric constraints posed by *two* phenyl neigbours in the *o*-position for three out of five terminal rings. A first casual statement concerning our coexistence of processes on vastly different time scales is that, considering the intriguing results for *o*-terphenyl, unusual findings should certainly not come as surprise. It seems difficult to reconcile the process in *o*-terphenyl with the restricted dynamics in the dendrimer. Apart from our "fast fraction", we can conclude that exact 180° flips are apparently suppressed to a large degree for terminal rings in the dendrimer. We hypothesize that the larger steric hindrance allows only for *concerted* reorientations of all terminal rings attached to one central ring. Carbon atoms in ortho or meta positions of the terminal rings therefore stay either above or below the central ring plane. The model is depicted at the top of Figure 10. This concertedness may further be the reason for our lower value for E_a (the inherent potential barrier is lower than for a 180° flip) and the not well-defined, but nevertheless rather low, values for k_0 (reduced overall rate due to low probability of a concerted flip). As we have seen in the comparison of regular dendrimers with the alkyl-substituted species (Figure 7c), the large difference in t_c must be due to a change in k_0, which in turn might vanish upon matrix solidification.

An unusual observation is the rather small reorientation angle of 24°. An angle of 52°, as derived from an average 26° tilt of terminal rings with respect to the central ring plane normal[54] under the assumption of concerted reorientation of all terminal rings connected to one central ring, seems more likely. However, assuming that the double para-substituted connecting ring cannot change its overall orientation due to steric constraints posed by more inner rings, a jump by 24° (or 26°) into a position where all but one rings stand almost perpendicular to the central ring might be an energetically favorable compromise. The existence of differing jump angles for the five adjacent rings could also be reconciled with the data. Further molecular modeling studies might provide a deeper insight into such fascinating concerted motions. Apart from these ambiguities, our conclusion of the existence of two-site jumps with an angle being substantially smaller than 90° and clearly different from 180° is beyond doubt.

3.3.2. Implications for Polyphenylene Dendrimer Structure. Leaving aside the complex molecular details of the dynamic processes, we have already concluded that the observation of generation-dependent changes in the intramolecular dynamics might imply arguments for the packing density of segments at the dendrimer periphery. To motivate our conclusions, we have plotted the fast fractions and slow exchange rates as a function of dendrimer generation (g) in parts a and b of Figure 12, respectively. In part c, we show crude graphs which predict the trend for the free volume (V_f) available to segments at the periphery of a spherical molecule and in the full volume based on the simple assumption that the number of phenyl rings grows exponentially with generation, while the available space grows with g^2 and g^3:

$$V_f(\text{surface}) \propto \frac{r^2}{N_{term}} \propto \frac{(1+2g)^2}{4 \times 2^{(g+1)}}$$

$$V_f(\text{sphere}) \propto \frac{r^3}{N_{tot}} \propto \frac{(1+2g)^3}{(5 \times (2^{(g+2)} - 4)) + 4}$$

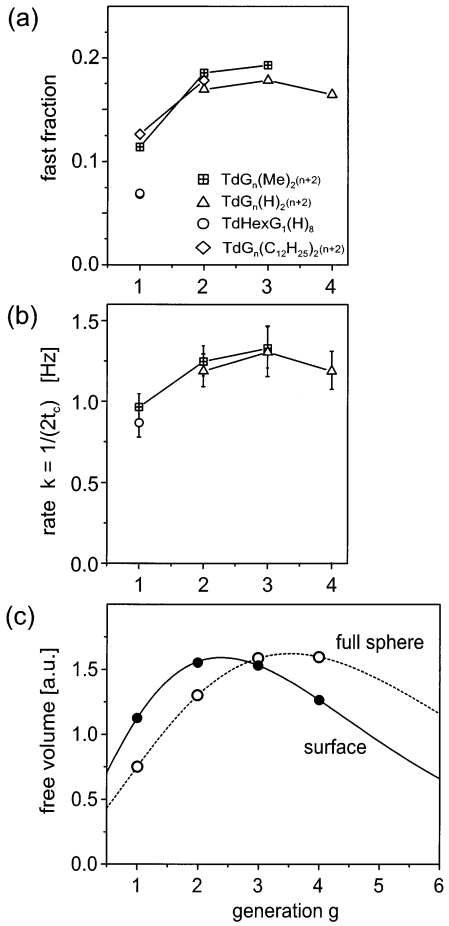

Figure 12. Tentative interpretation of the systemtatic generation-dependent trends observed for (a) the room temperature fraction of rapidly moving segments (reproduced from Figure 4a; the experimental error is on the order of the size of the symbols) and (b) the correlation times for the slow two-site process (discussed in section 3.2) at $T = 349$ K. In (c), the trends for the free volume available to terminal phenyl rings located at the dendrimer surface and all rings in an entire spherical volume are plotted as solid and dashed lines, respectively.

where, in the numerators, the sphere radius is given in "phenylene" units under the assumption of fully extended para conformation and, in the denominators, the exact number of phenyl rings is calculated (correct for $g \geq 1$). For V_f(surface), all terminal rings at the branch ends, excluding the central and the para-substituted connecting rings, are taken into account. Essentially the same scaling argument was brought forth by Maciejewski[27] when motivating the concept of topological trapping.

It is seen that both the fast fraction and the rates of the slow processes follow a trend that is intermediate between the behavior predicted by the evolution of surface and full-sphere free volume, respectively, with increasing dendrimer generation on average, irrespective of the surface substitution pattern of the dendrimer. Since both processes have been identified as being of intramolecular origin, we take the observed correlation as an argument in favor of an increasing surface density of segments and an accordingly increased sterical hindrance.

As a particularly strong indication for the effect of surface packing, the significant increase of average internal free volume of segments distributed over the

full sphere is still large upon going from the second to the third generation. This increase is not significantly reflected in the dynamic data. As can be derived from simple counting, the majority of terminal rings in each dendrimer (≈72% for $g > 1$) are located at the branch ends and, assuming extended arms, can be considered to be influenced by packing constraints at the periphery. It is therefore not surprising that the dynamics is dominated by surface packing. However, a fraction of terminal rings being located in the dendrimer interior and the participation of doubly para-substituted rings in the dynamics for higher generation give a possible explanation for the absence of a pronounced drop in the dynamic parameters upon going from the third to the fourth generation.

It is seen that the space available for surface segments first increases and decreases only for generations 3 and higher. Together with the knowledge that the scaffold is rigid and extended, this implies the existence of stable intramolecular cavities. Apart from the fact that the crystal structure of $TdHexG_1H_8$ (Figure 1d) indicates a rather open structure with solvent-filled voids,[54] independent experimental evidence of stable intramolecular voids can be inferred from PALS (positronium annihilation lifetime spectroscopy) studies[70] and the successful use of these dendrimers as specific small-molecule hosts in sensor applications using a quartz microbalance.[71] Finally, the strongest evidence in favor of a dense shell at higher generations can be taken from a neutron scattering study, which will be presented in an upcoming publication.[35]

We recall that de Gennes and Hervet's model for the structure of "starburst" molecules,[8] excluding backfolds, leads to a steadily decreasing segment free volume from the center to the periphery of the molecule. In contrast to our simpler argument, this behavior arises from their treatment of the radial growth variable as being continuous and from the more elaborate self-consistent-field model for the free energy. The model is not suited to describe low generations and extended arms. However, the proposed starburst limit as given by the physical limiting surface density of segments is observed for polyphenylene dendrimers: the synthesis of a perfect fifth-generation dendrimer is not possible any more.[31] This is corroborated by the trend curve for the surface fraction in Figure 12c, where V_f for generation 5 is smaller than for generation 1.

We have here presented the first experimental evidence for de Gennes' conclusion that "starburst structures are somewhat flexible in the early stages but quite rigid (at least in their outer surface) at [the starburst limit][8]." This "flexibility" cannot be considered to be dynamic in our system and is manifested only indirectly as a decrease of local steric hindrance and increased mobility of terminal rings at lower generations but can be directly inferred from simulations of the static structure of the second-generation dendrimer[34] and the possible formation of smectic layers of $TdG_2(C_{12}H_{25})_8$.[53,55] Both results agree in that a deformation of the scaffold toward a dumbbell shell shape with two paired arms extending in different directions is possible for G_2 but less favorable for higher generations.

Our results shall finally be compared with other solution[13,14] and solid-state[18−21] NMR studies of dynamics in regular, flexible dendrimers. Studies of ^{13}C and ^2H relaxation times in flexible polyamidoamine (PAMAM) dendrimers in solution[13,14] revealed increased mobility of chain termini, an overall decrease of mobility for both chain ends and interior sites as a function of generation, and no radial dependence of correlation times. This is consistent with a homogeneous decrease of segment free volume of the whole structure with increasing generation, which results from the possibility of backfolding upon dendrimer growth[10] and stands in pronounced contrast to our observations on shape-persistent dendrimers.

REDOR studies on distances between the core and the arm termini in poly(benzyl ether dendrimers)[18,19] as well as ^2H NMR investigations of dynamics in solid PAMAM dendrimer salts[20,21] consistently revealed the importance of backfolding at higher generations ($g > 4$) and the absence of indications of decreased segment free volume at the surface. In contrast, extensive arm interdigitation for generations ≤3 was identified as an important factor governing the distance estimates and the molecular dynamics. A balance between arm interdigitation at low generations and backfolding at higher generations was considered to be responsible for the observation of high mobility in the interior of third-generation PAMAM dendrimer salt.[20,21] This observation seems to superficially comply with our observations (Figure 12), but it must be emphasized that (i) our data are dominated by segments located close to the surface and (ii) interdigitation for lower-generation dendrimers does not play a significant role, as has been shown by comparing the crystalline and the amorphous modification of the $TdHexG_1H_8$ dendrimer (Figure 8).

All cited solid-state NMR studies were performed on dendrimers exhibiting broad glass transition ranges centered not far above ambient temperature, at which the crucial measurements were performed. Considering the richness and fascinating complexity of motional processes identified in the shape-persistent polyphenylene dendrimers, the physical properties of which clearly fulfill the usual definition of "far below T_g", great care must be taken when interpreting NMR data obtained on other dendrimers under conditions, where significant dynamics associated with T_g might complicate the situation even more. This is particularly true for intensity-based applications of recoupling methods such as REDOR,[43] where very undesirable interferences between the recoupling and intermediate motions can be expected.[68]

Acknowledgment. The authors are indebted to Detlef Reichert and Klaus Schmidt-Rohr for invaluable advice concerning the influence of spin diffusion on the exchange data, Robert Graf for recording some of the REPT spectra, and Michael Steiert for taking the X-ray powder spectra. U.M.W. is grateful for a scholarship from the Verband der Chemischen Industrie; K.S. thanks Prof. H Finkelmann for support and the Fonds der Chemischen Industrie for a habilitation grant. Financial aid by the Deutsche Forschungsgemeinschaft (SFBs 262 and 428) is gratefully acknowledged.

References and Notes

(1) Fischer, M.; Vögtle, F. Dendrimers: From Design to Application—A Progress Report. *Angew. Chem., Int. Ed.* **1999**, *38*, 884−905.
(2) Twyman, L. J.; Beezer, A. E.; Esfand, R.; Hardy, M. J.; Mitchell, J. C. The Synthesis of Water Soluble Dendrimers, and their Application as Possible Drug Delivery Systems. *Tetrahedron Lett.* **1999**, *40*, 1743−1746.
(3) Liu, M.; Fréchet, J. M. J. Designing Dendrimers for Drug Delivery. *Pharm. Sci. Technol. Today* **1999**, *2*, 393−401.

(4) Wiener, E. C.; Brechbiel, M. W.; Brothers, H.; Magin, R. L.; Gansow, O. A.; Tomalia, D. A.; Lauterbur, P. C. Dendrimer-based Metal Chelates: A New Class of Magnetic Resonance Imaging Contrast Agents. *Magn. Reson. Med.* **1994**, *31*, 1−8.
(5) Haensler, J.; Szoka, F. C., Jr. Polyamidoamine Cascade Polymers Mediate Efficient Transfection of Cells in Culture. *Bioconjugate Chem.* **1993**, *4*, 372−379.
(6) Ottaviani, M. F.; Furini, F.; Casini, A.; Turro, N. J.; Jockusch, S.; Tomalia, D. A.; Messori, L. Formation of Supramolecular Structures between DNA and Starburst Dendrimers Studied by EPR, CD, UV, and Melting Profiles. *Macromolecules* **2000**, *33*, 7842−7851.
(7) Kim, R. M.; Manna, M.; Hutchins, S. M.; Griffin, P. R.; Yates, N. A.; Bernick, A. M.; Chapman, K. T. Dendrimer-supported combinatorial chemistry. *Proc. Natl. Acad. Sci. U.S.A.* **1994**, *93*, 10012−10017.
(8) de Gennes, P. G.; Hervet, H. Statistics of "starburst" polymers. *J. Phys., Lett.* **1983**, *44*, 351−360.
(9) Naylor, A. M.; Goddard, W. A., III; Kiefer, G. E.; Tomalia, D. A. Starburst Dendrimers. 5. Molecular Shape Control. *J. Am. Chem. Soc.* **1989**, *111*, 2339−2341.
(10) Lescanec, R. L.; Muthukumar, M. Configurational Characteristics and Scaling Behavior of Starburst Molecules: A Computational Study. *Macromolecules* **1990**, *23*, 2280−2288.
(11) Murat, M.; Grest, G. S. Molecular Dynamics Study of Dendrimer Molecules in Solvents of Varying Quality. *Macromolecules* **1996**, *29*, 1278−1285.
(12) Boris, D.; Rubinstein, M. A Self-Consistent Mean Field Model of a Starburst Dendrimer: Dense Core vs Dense Shell. *Macromolecules* **1996**, *29*, 7251−7260.
(13) Meltzer, A. D.; Tirrell, D. A.; Jones, A. A.; Inglefield, P. T.; Hedstrand, D. M.; Tomalia, D. A. Chain Dynamics in Poly(amido amine) Dendrimers. A Study of ^{13}C NMR Relaxation Parameters. *Macromolecules* **1992**, *25*, 4541−4548.
(14) Meltzer, A. D.; Tirrell, D. A.; Jones, A. A.; Inglefield, P. T. Chain Dynamics in Poly(amido amine) Dendrimers. A Study of ^{2}H NMR Relaxation Parameters. *Macromolecules* **1992**, *25*, 4549−4552.
(15) Jansen, J. F. G. A.; de Brabander-van den Berg, E. M. M.; Meijer, E. W. Encapsulation of Guest Molecules into a Dendritic Box. *Science* **1994**, *266*, 1226−1229.
(16) Ottaviani, M. F.; Bossmann, S.; Turro, N. J.; Tomalia, D. A. Characterization of Starburst Dendrimers by the EPR Technique. 1. Copper Complexes in Water Solution. *J. Am. Chem. Soc.* **1994**, *116*, 661−671.
(17) Pötschke, D.; Ballauff, M.; Lindner, P.; Fischer, M.; Vögtle, F. Analysis of the Structure of Dendrimers in Solution by Small-Angle Neutron Scattering Including Contrast Variation. *Macromolecules* **1999**, *32*, 4079−4087.
(18) Wooley, K. L.; Klug, C. A.; Tasaki, K.; Schaefer, J. Shapes of Dendrimers from Rotational-Echo Double-Resoance NMR. *J. Am. Chem. Soc.* **1997**, *119*, 53−58.
(19) Kao, H.-M.; Stefanescu, A. D.; Wooley, K. L.; Schaefer, J. Location of Terminal Groups of Dendrimers in the Solid State by Rotational-Echo Double-Resonance NMR. *Macromolecules* **2000**, *33*, 6214−6216.
(20) Malyararenko, D. I.; Vold, R. L.; Hoatson, G. L. Solid State Deuteron NMR Studies of Polyamidoamine Dendrimer Salts. 1. Structure and Hydrogen Bonding. *Macromolecules* **2000**, *33*, 1268−1279.
(21) Malyararenko, D. I.; Vold, R. L.; Hoatson, G. L. Solid State Deuteron NMR Studies of Polyamidoamine Dendrimer Salts. 2. Relaxation and Molecular Motion. *Macromolecules* **2000**, *33*, 7508−7520.
(22) Chai, M.; Niu, Y.; Youngs, W. J.; Rinaldi, P. L. Structure and Conformation of DAB Dendrimers in Solution via Multidimensional NMR Techniques. *J. Am. Chem. Soc.* **2001**, *123*, 4670−4678.
(23) Ballauff, M. Structure of Dendrimers in Dilute Solution. *Top. Curr. Chem.* **2001**, *212*, 177−194.
(24) Buhleier, E.; Wehner, W.; Vögtle, F. "Cascade"- and "Nonskid-Chain-like" Syntheses of Molecular Cavity Topologies. *Synthesis* **1978**, *55*, 155−158.
(25) Tomalia, D. A.; Baker, H.; Dewald, J.; Hall, M.; Kallos, G.; Martin, S.; Roeck, J.; Ryder, J.; Smith, P. A New Class of Polymers: Starburst-Dendritic Macromolecules. *Polym. J.* **1985**, *17*, 117−132.
(26) Tomalia, D. A.; Baker, H.; Dewald, J.; Hall, M.; Kallos, G.; Martin, S.; Roeck, J.; Ryder, J.; Smith, P. Dendritic Molecules: Synthesis of Starburst Dendrimers. *Macromolecules* **1986**, *19*, 2466−2468.
(27) Maciejewski, M. Concepts of Trapping Topologically by Shell Molecules. *J. Macromol. Sci., Chem.* **1982**, *A17* (4), 689−703.
(28) Miller, T. M.; Neenan, T. X. Convergent Synthesis of Monodisperse Dendrimers Based upon 1,3,5-Trisubstituted Benzenes. *Chem. Mater.* **1990**, *2*, 346−349.
(29) Miller, T. M.; Neenan, T. X.; Zayas, R.; Blair, H. E. Synthesis and Characterization of a Series of Monodisperse, 1,3,5-Phenylene-Based Hydrocarbon Dendrimers Including C276H186 and their Fluorinated Analogues. *J. Am. Chem. Soc.* **1992**, *114*, 1018−1025.
(30) Morgenroth, F.; Kübel, C.; Müllen, K. Nanosized polyphenylene dendrimers based upon pentaphenylenebenzene units. *J. Mater. Chem.* **1997**, *7*, 1207−1211.
(31) Wiesler, U.-M.; Berresheim, A. J.; Morgenroth, F.; Lieser, G.; Müllen, K. Divergent Synthesis of Polyphenylene Dendrimers: The Role of Core and Branching Reagents upon Size and Shape. *Macromolecules* **2001**, *34*, 187−199.
(32) Wiesler, U.-M.; Weil, T.; Müllen, K. Nanosized Polyphenylene Dendrimers. *Top. Curr. Chem.* **2001**, *212*, 1−40.
(33) Zhang, H.; Grim, P. C. M.; Foubert, P.; Vosh, T.; Vanoppen, P.; Wiesler, U.-M.; Berresheim, A. J.; Müllen, K.; deSchryver, F. C. Properties of Single Dendrimer Molecules Studied by Atomic Force Microscopy. *Langmuir* **2000**, *16*, 9009−9014.
(34) Brocorens, P.; Zojer, E.; Cornil, J.; Shuai, Z.; Leising, G.; Müllen, K.; Brédas, J. L. Theoretical characterization of phenylene-based oligomers, polymers, and dendrimers. *Synth. Met.* **1999**, *100*, 141−162.
(35) Ballauff, M.; et al. In preparation.
(36) Wind, M.; Wiesler, U.-M.; Saalwächter, K.; Müllen, K.; Spiess, H. W. Shape-Persistent Polyphenylene Dendrimers—Restricted Molecular Dynamics from Advanced Solid-State NMR Techniques. *Adv. Mater.* **2001**, *13*, 752−756.
(37) Schmidt-Rohr, K.; Spiess, H. W. *Multidimensional Solid-State NMR and Polymers;* Academic Press: London, 1994.
(38) Schnell, I.; Spiess, H. W. High-Resolution ^{1}H NMR Spectroscopy in the Solid State: Very-Fast Sample Rotation and Multiple-Quantum Coherences. *J. Magn. Reson./Adv. Magn. Reson.* **2001**, *151*, 153−227.
(39) Brown, S. P.; Spiess, H. W. Advanced Solid-State NMR Methods for the Elucidation of Structure and Dynamics of Molecular, Macromolecular, and Supramolecular Systems. *Chem. Rev.* **2001**, *101*, 4125−4155.
(40) Filip, C.; Hafner, S.; Schnell, I.; Demco, D. E.; Spiess, H. W. Solid-state nuclear magnetic resonance spectra of dipolar-coupled multi-spin systems under fast magic angle spinning. *J. Chem. Phys.* **1999**, *110*, 423−440.
(41) Munowitz, M.; Griffin, R. G. Two-dimensional nuclear magnetic resonance in rotating solids: An analysis of line shapes in chemical shift-dipolar spectra. *J. Chem. Phys.* **1982**, *76*, 2848−2858.
(42) McElheny, D.; DeVita, E.; Frydman, L. Heteronuclear Local Field NMR Spectroscopy under Fast Magic-Angle Sample Spinning Conditions. *J. Magn. Reson.* **2000**, *143*, 321−328.
(43) Gullion, T.; Schaefer, J. Rotational-Echo Double-Resonance NMR. *J. Magn. Reson.* **1989**, *81*, 196−200.
(44) Hing, A. W.; Vega, S.; Schaefer, J. Transferred-Echo Double-Resonance NMR. *J. Magn. Reson.* **1992**, *96*, 205−209.
(45) Saalwächter, K.; Graf, R.; Spiess, H. W. Recoupled Polarization Transfer Heteronuclear ^{1}H-^{13}C Multiple-Quantum Correlation in Solids under Ultra-fast MAS. *J. Magn. Reson.* **1999**, *140*, 471−476.
(46) Friedrich, U.; Schnell, I.; Brown, S. P.; Lupulescu, A.; Demco, D. E.; Spiess, H. W. Spinning-sideband patterns in multiple-quantum magic-angle spinning NMR spectroscopy. *Mol. Phys.* **1998**, *95*, 1209−1227.
(47) Saalwächter, K.; Graf, R.; Spiess, H. W. Recoupled Polarization-Transfer Methods for Solid-State ^{1}H-^{13}C Heteronuclear Correlation in the Limit of Fast MAS. *J. Magn. Reson.* **2001**, *148*, 398−418.
(48) Saalwächter, K.; Spiess, H. W. Heteronuclear ^{1}H-^{13}C multiple-spin correlation in solid-state NMR: combining REDOR recoupling and multiple-quantum spectroscopy. *J. Chem. Phys.* **2001**, *114*, 5707−5728.
(49) deAzevedo, E. R.; Hu, W.-G.; Bonagamba, T. J.; Schmidt-Rohr, K. Centerband-Only Detection of Exchange: Efficient Analysis of Dynamics in Solids by NMR. *J. Am. Chem. Soc.* **1999**, *121*, 8411−8412.
(50) deAzevedo, E. R.; Hu, W.-G.; Bonagamba, T. J.; Schmidt-Rohr, K. Principles of centerband-only detection of exchange in solid-state nuclear magnetic resonance, and extension to four-time centerband-only detection of exchange. *J. Chem. Phys.* **2000**, *112*, 8988−9001.
(51) Metz, G.; Wu, X.; Smith, S. O. Ramped-Amplitude Cross Polarization in Magic-Angle-Spinning NMR. *J. Magn. Reson. A* **1994**, *110*, 219−227.

(52) Langer, B.; Schnell, I.; Spiess, H. W.; Grimmer, A.-R. Temperature calibration under ultrafast MAS conditions. *J. Magn. Reson.* **1999**, *138*, 182−186.
(53) Wiesler, U.-M. Charakterisierung und Funktionalisierung von Polyphenylen-Dendrimeren. Dissertation, Universität Mainz, 2001.
(54) Bauer, R. E.; Enkelmann, V.; Wiesler, U.-M.; Berresheim, A. J.; Müllen, K. Single-Crystal Structures of Polyphenylene Dendrimers. *Chem. Eur. J.* **2002**, *8*, 3858−3864.
(55) Loi, S.; Wiesler, U.-M.; Butt, H.-J.; Müllen, K. Self-Assembly of Alkyl-Substituted Polyphenylene Dendrimers on Graphite. *Macromolecules* **2001**, *34*, 3661−3671.
(56) Gédéon, A.; Favre, D. E.; Reichert, D.; MacNeil, J.; Chmelka, B. F. Distributions of Site-Hopping Geometries and Rates for Benzene Adsorbed on Ag−Y Zeolite. *J. Phys. Chem. A* **1999**, *103*, 6691−6703.
(57) Reichert, D.; Hempel, G.; Poupko, R.; Luz, Z.; Olejniczak, Z.; Tekely, P. MAS NMR studies of carbon-13 spin exchange in durene. *Solid State NMR* **1998**, *13*, 137−148.
(58) Reichert, D.; Bonagamba, T. J.; Schmidt-Rohr, K. Slow-Down of ^{13}C Spin Diffusion in Organic Solids by Fast MAS: A CODEX NMR Study. *J. Magn. Reson.* **2001**, *151*, 129−135.
(59) Wilhelm, M.; Spiess, H. W. Detection of Slow 180° Phenylene Flips in PET Fibers via ^{13}C Two-Dimensional Solid-State Exchange NMR. *Macromolecules* **1996**, *29*, 1088−1090.
(60) Wehrle, M.; Hellmann, G. P.; Spiess, H. W. Phenylene motion in polycarbonate and polycarbonate/additive mixtures. *Colloid Polym. Sci.* **1987**, *265*, 815−822.
(61) Liu, S.-F.; Mao, J.-D.; Schmidt-Rohr, K. A Robust Technique for Two-Dimensional Separation of Undistorted Chemical-Shift Anisotropy Powder Patterns in Magic-Angle-Spinning NMR. *J. Magn. Reson.* **2002**, *155*, 15−28.
(62) Fischbach, I.; Saalwächter, K.; Pakula, T.; Minkin, P.; Fechtenkötter, A.; Müllen, K.; Spiess, H. W. Structure and dynamics in columnar discotic materials: A combined X-ray and solid-state NMR study of hexabenzocoronene derivatives. *J. Phys. Chem. B* **2002**, *106*, 6408−6418.
(63) Veeman, W. S. Carbon-13 Chemical Shift Anisotropy. *Prog. NMR Spectrosc.* **1983**, *16*, 193−2351.
(64) Bonagamba, T. J.; Becker-Guedes, F.; DeAzevedo, E. R.; Schmidt-Rohr, K. Slow Ester Side-Group Flips in Glassy Poly(alkyl methacrylate)s Characterized by Centerband-Only Detection of Exchange Nuclear Magnetic Resonance. *J. Polym. Sci., Part B: Polym. Phys.* **2001**, *39*, 2444−2453.
(65) Barich, D. H.; Pugmire, R. J.; Grant, D. M.; Iuliucci, R. J. Investigation of the Structural Conformation of Biphenyl by Solid State ^{13}C NMR and Quantum Chemical NMR Shift Calculations. *J. Phys. Chem. A* **2001**, *105*, 6780−6784.
(66) Ochsenfeld, C.; Brown, S. P.; Schnell, I.; Gauss, J.; Spiess, H. W. Structure Assignment in the Solid State by the Coupling of Quantum Chemical Calculations with NMR Experiments: A Columnar Hexabenzocoronene Derivative. *J. Am. Chem. Soc.* **2001**, *123*, 2597−2606.
(67) Leisen, J.; Werth, M.; Boeel, C.; Spiess, H. W. Molecular dynamics at the glass transition: One-dimensional and two-dimensional nuclear magnetic resonance studies of a glass-forming discotic liquid crystal. *J. Chem. Phys.* **1992**, *97*, 3749−3759.
(68) Saalwächter, K.; Fischbach, I. The Application of MAS Recoupling Methods in the Intermediate Motional Regime. *J. Magn. Reson.* **2002**, *157*, 17−30.
(69) Stumber, M.; Zimmermann, H.; Schmitt, H.; Haeberlen, U. *o*-Terphenyl: flips of the end rings in the crystal phase. *Mol. Phys.* **2001**, *99*, 1091−1098.
(70) Süvegh, K.; Marek, T.; Vértes, A.; Weil, T.; Bauer, R. E.; Wiesler, U.-M.; Klapper, M.; Müllen, K. Stable Voids in Polyphenylene Dendrimers. In preparation.
(71) Schlupp, M.; Weil, T.; Berresheim, A. J.; Wiesler, U. M.; Müllen, K. Polyphenylene Dendrimers as Sensitive and Selective Sensor Layers. *Angew. Chem., Int. Ed.* **2001**, *40*, 4011−4015.

MA021283D